NASA Technical Memorandum 87097

Elastohydrodynamic Lubrication Calculations Used as a Tool to Study Scuffing

L.G. Houpert and B.J. Hamrock
Lewis Research Center
Cleveland, Ohio

Prepared for the
12th Leeds-Lyon Symposium on Tribology
Lyon, France, September 3-6, 1985

NASA

L.G. Houpert and B.J. Hamrock

Elastohydrodynamic Lubrication Calculations Used as a Tool to Study Scuffing

A new Reynolds equation is developed that takes into account the nonlinear viscous behavior of the fluid. The new Reynolds equation considers the nonlinear viscous fluid model of Eyring, the equilibrium equation, the constant mass flow, and the kinematic boundary condition. The new Reynolds equation and the elasticity equation are solved simultaneously by using a system approach and a Newton-Raphson technique. Comparisons are made with results obtained from the classical Reynolds equation. The effects of sliding speed and introducing a bump or a groove within the conjunction are studied. Results are shown for both moderate and heavy loads.

1 INTRODUCTION

Scuffing is a problem encountered mainly in gears and rolling-element bearings. In rolling-element bearings, for example, scuffing is found in the acceleration zone of large bearings that are heavily loaded. For these circumstances, inertia effects probably lead to high sliding speeds. The authors feel that scuffing is related to

(1) Film thickness failure of the macro-contacts, as studied by Dyson (1976), and the microcontacts
(2) High pressure and shear stresses acting on the surface
(3) High surface temperatures found when sliding speeds are high

Film thickness failures lead to metal-to-metal contact; high surface stresses lead to rolling bearing fatigue, as studied by Ioannides an Harris (1985); and high surface temperatures may cause local melting of the surfaces.

Since the surface temperature can be calculated if the kinematic and surface stresses are known, important parameters to control when studying scuffing are film thickness and surface stresses. These parameters can be calculated by using elastohydrodynamic lubrication (EHL) analysis. In the present paper, a new method is described to study macro- and micro-EHL without any restriction on the load applied to the contact. By macro-EHL, we mean the lubricant film thickness developed in the inlet zone of the EHL conjunction. Micro-EHL may occur below the asperities and is due to the squeeze or sliding speed effects of the bearing as described by Cheng (1983). Macro-EHL is first studied by using the classical Reynolds equation (linear viscous fluid model), and the results are shown to be accurate for any applied loads. But under the severe conditions mentioned above (large pressure and high sliding speeds), the lubricant behavior can no longer be considered to be linear viscous, and a nonlinear viscous model is developed. With this fluid model, a modified or new Reynolds equation is derived. The new Reynolds equation and the elasticity equations are solved simultaneously by using a system approach and a Newton-Raphson technique. Film thickness, pressure, and shear stress can be obtained without any load restriction. The method described herein is therefore a very powerful tool that can be used in studying scuffing. To illustrate the power of the new approach, stress concentrations near a bump and a groove are studied.

1.1 Symbols

A dimensionless sliding speed, $(u_b - u_a)/u_a$

b half Hertzian width, $R\sqrt{8W/\pi}$, m

b' half-width of singularity, m

C_1 constant, $2E'W/\pi_{o,ref}$

C_2 constant, $\pi EU/8W\pi_{o,ref}$

C_j weight factors used to integrate P

E modulus of elasticity, N/m^2

E' effective elastic modulus, $2\left[(1 - \nu_a^2)/E_a + (1 - \nu_b^2)/E_b)\right]^{-1}$, N/m^2

G dimensionless materials parameter, $\alpha E'$

H dimensionless film thickness, $hR/b^2 = \pi h/8RW$

H_e dimensionless film thickness when $dP/dX = 0$

H_0 dimensionless constant used in calculation of H

h film thickness, m

i,j nodes

K constant, $3\pi^2U/4W^2$

N number of nodes used in linear system

P dimensionless pressure, p/p_H

p pressure, N/m^2

p_H maximum Hertzian pressure, $E'b/4R$, N/m^2

R equivalent radius, $(1/r_a + 1/r_b)^{-1}$, m

r curvature radius, m

S $\eta u_a/h\tau_0 = C_2\,\bar{\eta}/H\bar{\tau}_0\,(1 + A/2)$

T $(h/\tau_0)\,dp/dx = C_1(H/\bar{\tau}_0)(dP/dX)$

U dimensionless speed parameter, $\eta_0\bar{u}/E'R$

u velocity of fluid

$\bar{u}$ mean velocity, $(u_a + u_b)/2$

W dimensionless load, $w/E'R$

w applied load per unit length, N/m

X dimensionless abscissa, xR/b^2

x abscissa along rolling direction, m

x_p position of singularity

Z dimensionless coordinate, z/h

z coordinate in direction of film thickness, m

z_m height of singularity, m

α pressure–viscosity coefficient of fluid, m^2/N

$\dot{\gamma}$ strain rate, s^{-1}

η viscosity of fluid, $N\,s/m^2$

$\bar{\eta}$ dimensionless viscosity, η/η_0

η_0 viscosity at atmospheric pressure, $N\,s/m^2$

μ^R traction coefficient due to rolling speed

μ^S traction coefficient due to sliding speed

ν Poisson's ratio

ρ density of lubricant, kg/m^3

$\bar{\rho}$ dimensionless density, ρ/ρ_0

ρ_e density when $dp/dx = 0$, kg/m^3

ρ_0 density at atmospheric pressure, kg/m^3

τ shear stress, N/m^2

τ_0 critical shear stress, N/m^2

$\bar{\tau}_0$ dimensionless critical shear stress, $\tau_0/\tau_{0,ref}$

2 CLASSICAL REYNOLDS SOLUTION

From Houpert and Hamrock (1985), the integrated, dimensionless form of the classical Reynolds equation may be written as

$$H^3\frac{dP}{dX} = K\bar{\eta}\left(H - \frac{\rho_e H_e}{\rho}\right) \qquad (1)$$

where

$$\left.\begin{aligned} K &= \frac{3\pi^2}{4}\frac{U}{W^2}, \quad U = \frac{\eta_0\bar{u}}{E'R}, \quad W = \frac{w}{E'R} \\ P &= \frac{p}{p_H}, \quad X = \frac{x}{b}, \quad H = \frac{hR}{b^2}, \quad \bar{\eta} = \frac{\eta}{\eta_0} \end{aligned}\right\} \qquad (2)$$

Conventional solution of equation (1) required large computer run time, and the approach failed at moderate and high loads. Okamura (1982) used a system approach in solving equation (1). Houpert and Hamrock (1985) improved on Okamura's approach by making the following changes:

(1) Used a nonuniform mesh to improve the accuracy of the calculations in the pressure spike region and in the inlet
(2) Used a more accurate way of calculating the elasticity
(3) Solved for pressure difference rather than actual pressures
(4) Used Roelands' pressure–viscosity model

By incorporating these changes, Houpert and Hamrock (1985) were able to get accurate and fast solutions without any restriction on load. Figure 1 illustrates how fast the new approach is. It gives the pressure and film profiles at iterations 0, 1, and 14. Note that in the first iteration a pressure spike was formed that is close to the final converged pressure spike. In general, it took about 15 iterations to obtain a converged solution, or about 2 min of CPU time on an IBM 370 computer with a mesh of 181 nodes. Compare this with the 100 min normally taken by the Hamrock and Jacobson (1984) approach.

Figure 2 shows the pressure profile and film thickness ratio for five dimensionless loads varying over two orders of magnitude. This dimensionless load range corresponds to a maximum Hertzian pressure of 0.4 to 4.8 GPa, which is well within the range that rolling-element bearings and gears experience. As the load increases (Fig. 2(a)), the pressure spike becomes smaller and moves toward the outlet. Furthermore, as the load increases, the inlet meniscus moves toward the abscissa $X = -1$. The nip film thickness width and length (Fig. 2(b)) both decrease as the load increases.

3 NEW REYNOLDS EQUATION

The classical Reynolds equation (1) has been obtained by assuming the lubricant behavior to be linear viscous. This is only true at low pressures, or high temperatures, and when the shear rates are small. A more appropriate lubricant rheological model is the Eyring (1936) nonlinear viscous model used by Hirst and Moore (1974), Johnson and Greenwood (1980), and Berthe et al. (1978 and 1979). Elastic viscous models have also been used by Johnson and Tevaarwerk (1977), Bair and Winer (1978), Berthe et al. (1979), Houpert et al. (1981), and Houpert (1985a), but elastic effects have been shown to be often negligible as proposed by Houpert (1985b).

The Eyring (1936) model will therefore be used to develop a new Reynolds equation. The new Reynolds equation will assume an isothermal behavior and neglect transient and squeeze-film effects. However, the new rheological model,

equilibrium equation, boundary kinematic conditions, and constant mass flow conditions have been taken into account.

From equilibrium, we can write that

$$\frac{dp}{dx} = \frac{d\tau}{dz} \tag{3}$$

Integrating gives

$$\frac{\tau}{\tau_o} = \frac{z}{\tau_o}\frac{dp}{dx} + \frac{A_1}{\tau_o} \tag{4}$$

where A_1 is a constant to be defined later. Erying's (1936) nonlinear viscous fluid model can be expressed as

$$\dot{\gamma} = \frac{du}{dz} = \frac{\tau_o}{\eta}\sinh\left(\frac{\tau}{\tau_o}\right) \tag{5}$$

Substituting equation (4) into equation (5) gives

$$\frac{du}{dz} = \frac{\tau_o}{\eta}\sinh\left(\frac{z}{\tau_o}\frac{dp}{dx} + \frac{A_1}{\tau_o}\right) \tag{6}$$

Integrating gives

$$u = \frac{\tau_o}{\eta}\cosh\left(\frac{z}{\tau_o}\frac{dp}{dx} + \frac{A_1}{\tau_o}\right)\frac{\tau_o}{\left(\frac{dp}{dx}\right)} + A_2 \tag{7}$$

where A_2 is an integration constant. The boundary conditions are

(i) $z = 0, \quad u = u_a$

(ii) $z = h, \quad u = u_b$

By making use of these boundary conditions, the constants A_1 and A_2 are defined and we find that

$$\frac{u}{u_a} = 1 + \frac{1}{ST}\left[\cosh\left(ZT + \frac{A_1}{\tau_o}\right) - \cosh\left(\frac{A_1}{\tau_o}\right)\right] \tag{8}$$

where

$$\frac{A_1}{\tau_o} = \sinh^{-1}\left[\frac{AST}{2\sinh\left(\frac{T}{2}\right)}\right] - \frac{T}{2} \tag{9}$$

$$\left.\begin{aligned} A &= \frac{u_b - u_a}{u_a}, \quad Z = \frac{z}{h}, \\ S &= \frac{\eta u_a}{\tau_o h} = \frac{C_2}{\left(1 + \frac{A}{2}\right)}\frac{\bar{\eta}}{H\bar{\tau}_o} \\ T &= \frac{h}{\tau_o}\frac{dp}{dx} = C_1\frac{H}{\bar{\tau}_o}\frac{dP}{dX} \end{aligned}\right\} \tag{10}$$

Making use of equations (9) and (10), we can rewrite equations (4) and (6) as

$$\frac{\tau}{\tau_o} = \sinh^{-1}\left[\frac{AST}{2\sinh\frac{T}{2}}\right] + T(Z - 0.5) \tag{11}$$

$$\frac{d}{dZ}\left(\frac{u}{u_a}\right) = \frac{1}{S}\sinh\left\{T(Z - 0.5) + \sinh^{-1}\left[\frac{AST}{2\sinh\frac{T}{2}}\right]\right\} \tag{12}$$

To calculate the mass flow, it is convenient to express the velocity distribution as

$$\frac{u}{u_a} = 1 + A + \frac{2}{ST}\sinh\left[\frac{T}{2}(Z - 1)\right] \times \sinh\left\{\frac{TZ}{2} + \sinh^{-1}\left[\frac{AST}{2\sinh\left(\frac{T}{2}\right)}\right]\right\} \tag{13}$$

Note from equation (13) that when $dp/dx \to 0$, then $T \to 0$, $\sinh(T/2)/(T/2) \to 1$, and $\sinh[T/2(Z - 1)]/(T/2) \to (Z - 1)$. Therefore

$$\frac{u}{u_a} = 1 + AZ \quad \text{when} \quad T \to 0 \tag{14}$$

The mass flow when $dp/dx = 0$ can be written as

$$\int_0^1 \rho_e h_e\left(\frac{u}{u_a}\right)dZ = \rho_e h_e\int_0^1 (1 + AZ)\,dZ = \rho_e h_e\left(1 + \frac{A}{2}\right) \tag{15}$$

The condition of constant mass flow at any location can therefore be written as

$$\rho_e h_e\left(1 + \frac{A}{2}\right) = \rho h\int_0^1\left(\frac{u}{u_1}\right)dZ$$

Making use of equation (13) gives

$$\left(1 + \frac{A}{2}\right)\left(\frac{\rho_e h_e}{\rho h} - 1\right) = \frac{1}{ST}\left\{1 + \left[\frac{AST}{2\sinh\left(\frac{T}{2}\right)}\right]^2\right\}^{1/2} \times \left[\frac{2}{T}\sinh\left(\frac{T}{2}\right) - \cosh\left(\frac{T}{2}\right)\right] \tag{16}$$

Equation (16) is the new Reynolds equation. But in order to make a comparison with the linear viscous equation, equation (16) must be rewritten as

$$H^3\frac{dP}{dX} = \frac{K\bar{\eta}\left(H - \frac{\rho_e H_e}{\rho}\right)}{\left\{1 + \left[\frac{\frac{AST}{2}}{\sinh\left(\frac{T}{2}\right)}\right]^2\right\}^{1/2}} - e \tag{17}$$

where

$$e = -\frac{6\pi H^2 \tau_0}{E' WT}\left[\frac{2}{T}\sinh\left(\frac{T}{2}\right) - \cosh\left(\frac{T}{2}\right) + \frac{T^2}{12}\right] \quad (18)$$

Comparing equation (1) with equation (17) indicates quite clearly the contribution due to the nonlinear fluid model.

Table I shows the difference in the equations developed for the nonlinear and linear viscous fluid models. Note that if $\tau_0 \to \infty$, then $T \to 0$, $e \to 0$, and $S \to 0$. For this situation the nonlinear viscous equation reduces to the linear viscous equation. Therefore, the new Reynolds equation to be solved at each node in dimensionless form can be expressed as

$$f_i = H_i^3\left(\frac{dP}{dX}\right)_i - \frac{K\bar{n}_i\left(H_i - \frac{\rho_e H_e}{\rho_i}\right)}{\left\{1 + \left[\frac{AS_iT_i}{2\sinh\left(\frac{T_i}{2}\right)}\right]^2\right\}^{1/2}} + e_i = 0 \quad (19)$$

4 SYSTEM SOLUTION

The basic equation to solve at each node i is the new Reynolds equation given in equation (19) or $f_i = 0$, where f is a function of $\bar{\rho}_e H_e$, H_0, and the pressures P_2 to P_N. The expression for f also contains the dimensionless film thickness H, which is expressed as

$$H_i = H_0 + \frac{X_i^2}{2} + \sum_{j=1}^{N} D_{ij}P_j + \frac{R}{b^2}g(x) \quad (20)$$

where $g(x)$ defines the microgeometry. The numerical approach used to solve the system of equations $f_i = 0$ is identical to the one used by Houpert and Hamrock (1985). A Newton-Raphson technique is used and leads to the solution of a linear system of equations where a Jacobian matrix has to be calculated as a function of the Jacobian elements $\partial f_i/\partial(\bar{\rho}_e H_e)$, $\partial f_i/\partial P_j$, and $\partial f_i/\partial H_0$. A linear system of $N + 1$ equations is solved

$$\begin{bmatrix} \frac{\partial f_1}{\partial(\bar{\rho}_e H_e)} & \frac{\partial f_1}{\partial P_2} & \cdots & \frac{\partial f_1}{\partial P_N} & \frac{\partial f_1}{\partial H_0} \\ \frac{\partial f_2}{\partial(\bar{\rho}_e H_e)} & \frac{\partial f_2}{\partial P_2} & \cdots & \frac{\partial f_2}{\partial P_N} & \frac{\partial f_2}{\partial H_0} \\ \vdots & \vdots & & \vdots & \vdots \\ \frac{\partial f_N}{\partial(\bar{\rho}_e H_e)} & \frac{\partial f_N}{\partial P_2} & \cdots & \frac{\partial f_N}{\partial P_N} & \frac{\partial f_N}{\partial H_0} \\ 0 & C_2 & \cdots & C_N & 0 \end{bmatrix} \begin{Bmatrix} \Delta(\bar{\rho}_e H_e) \\ \Delta(P_2) \\ \vdots \\ \Delta(P_N) \\ \Delta(H_0) \end{Bmatrix} = \begin{Bmatrix} -f_1 \\ -f_2 \\ \vdots \\ -f_N \\ \Delta W \end{Bmatrix} \quad (21)$$

where C_i are the integration coefficients developed in Houpert and Hamrock (1985) and ΔW is a parameter representative of the constant load. The Jacobian elements are given in the appendix. The unknowns of the system are ΔP_j, $\Delta(\bar{\rho}_e H_e)$, and ΔH_0; they must be less than or equal to, respectively, 1/1000 of P_j, $\bar{\rho}_e H_e$, and H_0. More details on handling the exit boundary and, in general, how the system approach is used are covered in Houpert and Hamrock (1985) and will not be repeated here.

In general, 10 to 15 iterations are required for convergence of the results and only 2 min of CPU time are necessary on the IBM 370. This approach is therefore very fast, powerful, and relatively easy to program. As a result of the calculations, the film thickness H_i and pressure P_i are known at every node. Furthermore, the shear stress τ, the shear rate $\partial u/\partial z$, and the velocity u are known for values across the film.

5 DISCUSSION AND RESULTS

Maintaining a fluid film of adequate magnitude is an essential feature for the correct operation of lubricated machine elements. Results presented in this section make use of the nonlinear viscous rheological model of the lubricant and apply surface irregularities such as bumps and grooves to illustrate the possibilities of the new approach.

We first determined whether there was any difference between the film thickness obtained from the new Reynolds equation and that obtained from the classical Reynolds formulation. From disk machine experiments and traction force calculations, τ_0 has often been found to increase linearly with pressure. But at high pressure, a limiting value $\tau_{0,\ell}$ is found as proposed by Houpert (1985b) and Ten Napel et al. (1985). A possible relationship can be written as

$$\frac{\tau_0}{\tau_{0,\ell}} = \frac{\tau_{0,\mathrm{ref}}\,\bar{\tau}_0}{\tau_{0,\ell}} = 1 - \exp\left(-\frac{ap}{\tau_{0,\ell}}\right) + \varepsilon$$

where a and $\tau_{0,\ell}$ are defined for each lubricant as a function of the temperature. The term ε is very small (10^{-3}) and is introduced to avoid numerical problems when calculating $1/\tau_0$ as $p \to 0$.

Numerical runs have been performed with $a = 2.6\times10^{-2}$ and $\tau_{0,\mathrm{ref}} = \tau_{0,\ell} = 1.7\times10^{7}$ Pa that show some small numerical instabilities at the outlet of the contact while the film thickness is essentially a function of the inlet as clearly indicated by Houpert and Hamrock (1985) in their pressure spike analysis. The results obtained indicate clearly that the film thicknesses for the two forms of the Reynolds equation were identical for the conditions simulated here (i.e., $U = 1\times10^{-11}$, $G = 5007$, and $W = 2\times10^{-5}$). The reason for this is that the shear stress was smaller than τ_0 in the inlet zone. Since the film thickness is established by the hydrodynamic action in the inlet region and this was not altered by the new form of the Reynolds equation, the film shape did not change much. Because of this result and to avoid numerical instabilities, τ_0 will be assumed to be constant ($\tau_0 = \tau_{0,\ell}$; $\bar{\tau}_0 = 1$) in what follows. But it should be mentioned that, in general, accurate film thickness calculations require the knowledge of τ_0 at very small pressures although τ_0 has always been

determined at large pressure for traction forces calculations.

The effect of dimensionless sliding speed A on pressure and film shape through the lubricating conjunction is shown in Fig. 3. The sliding speed had little effect on film thickness but a significant effect on the definition of the pressure spike. As the sliding speed increased, the pressure spike diminished. The main reason for the change in pressure spike with sliding speed was that near the pressure spike the shear stress was larger than τ_0. The rolling traction coefficient μ^R remained almost unchanged ($\mu^R = 4.4\times10^{-4}$) while the sliding traction coefficient μ^S increased from 0 to 8.4×10^{-2} when A increased from 0 to 10.

Having shown some results of using the new Reynolds equation, the next task was to prestudy micro-EHL. As a first step and example of application of the tool presented herein, we were interested in what effect a bump or groove has on the film shape and stress concentration. The change of shape due to a bump or groove is taken care of by g(x) in the film shape equation (20). For simplicity, g(x) is a polynomial of degree 2 described as a function of the singularity half-width b', position x_p, and maximum height z_m, which is positive for a groove and negative for a bump.

$$g(x) = z_m \left[1 - \left(\frac{x - x_p}{b'}\right)^2\right] \quad \text{for } |x - x_p| \leq b'$$

$$= 0 \quad \text{for } |x - x_p| > b'$$

In what follows, b' is equal to 0.25×10^{-4} m and z_m to -0.1×10^{-6} m for the bump and 2×10^{-6} m for the groove. These values are to be compared with the equivalent roller radius $R = 0.111125\times10^{-1}$ m and the Hertzian half-width $b = 0.8\times10^{-4}$ m at moderate load ($W = 2\times10^{-5}$). The central film thickness value h in a smooth situation is 0.25×10^{-6} m. A large sliding speed, A = 10, has been imposed.

Figure 4 shows the film shape and pressure profile when a bump occurs in the inlet region of the conjunction ($x_p = -0.1\times10^{-3}$ m = -1.25 b). The undeformed and deformed shapes of the bump are presented. This figure shows that the bump occurring in the inlet region had quite an effect on the level of the film thickness but did not alter the film shape appreciably. The film thickness was less with the bump than without. The bump also moved the pressure spike toward the outlet and lowered the spike height. The coefficients μ^R and μ^S were slightly affected by the bump ($\mu^R = 6\times10^{-4}$ and $\mu^S = 8.56\times10^{-2}$).

Figure 5 shows the effect of a bump in the center of the conjunction on the pressure and film shape. The bump was the same as that used in Fig. 4, but its location was changed ($x_p = 0$). When the bump was in the center, there was no difference in minimum film thickness. Recall from Fig. 4 that the bump did significantly affect film thickness when it was located in the inlet region. Furthermore, Fig. 5 shows that the presence of the bump in the center of the contact had a profound effect on the pressure profile. Stress concentrations p/p_H of the order of 1.5 were calculated. Also the shape of the bump changed considerably in going from the undeformed state to the deformed state. This was not found when the bump was located in the inlet region (Fig. 4). The coefficients μ^R and μ^S remained almost unchanged ($\mu^R = 4.9\times10^{-6}$, $\mu^S = 8.5\times10^{-2}$).

The effect of a groove is shown in Figs. 6 and 7. The depth of the groove had to be made 20 times that of the bump used in Figs. 4 and 5 in order to get a comparable effect on pressure and film shape. Therefore, a groove would have considerably less effect on pressure and film shape than a bump if the bump and groove each had the same depth and width. Figure 6 shows the groove in the inlet, and Fig. 7 shows the groove in the center of the contact. The observations made for a bump in the inlet and in the center of the contact can also be made about a groove, but substantial differences were noted concerning μ^R and μ^S. When the groove was in the inlet, $\mu^R = 7.5\times10^{-4}$ and $\mu^S = 9.6\times10^{-2}$ as compared with $\mu^R = 3.98\times10^{-3}$ and $\mu^S = 7.89\times10^{-2}$ when the groove was in the center. Although temperature effects have been neglected in this study, the increase of μ^S when the groove was in the inlet can be easily related to the experimental results of Cusano and Wedeven (1983), who found similar increases in μ^S.

The results presented thus far are for a moderate load. Figures 8 and 9 are for a heavy load ($W = 3\times10^{-3}$). At this heavy load, $b = 0.97\times10^{-3}$ m and $h = 0.89\times10^{-8}$ m; $b' = 1.94\times10^{-4}$ m (or 0.2 b) and $z_m = 1.48\times10^{-6}$ m (or 16.6 h) for the groove and -1.43×10^{-7} m (or -1.6 h) for the bump. The sliding speed A was fixed at 0.1. Figure 8 shows the effect of a bump and Fig. 9 shows the effect of a groove, respectively, at positions x_p of 0.4 b and 0.2 b. The shapes of the bump and groove changed considerably once elastic deformation was considered. The pressure profile for the bump was very much Hertzian except at the corners of the bump. Stress concentrations were calculated for the groove only, but it should be remembered that the groove was 10 times deeper than the bump. The coefficient μ^R was found to be almost nil ($\mu^R = 6.6\times10^{-7}$) while μ^S was found in the two cases to equal 11.4×10^{-2}. This large value was due to the isothermal assumption.

6 CONCLUSIONS

A new Reynolds equation was developed that takes into account the nonlinear viscous behavior of the fluid. The new Reynolds equation and the elasticity equation were solved simultaneously by using a system approach and a Newton-Raphson technique. The film thickness was identical to that calculated by using the classical Reynolds equation (assuming a linear viscous fluid model). The pressure spike decreased as the sliding speed increased. A bump or groove in the inlet had a more significant effect than if it was located at the center of the contact. The effect of a bump on pressure and film thickness was more significant than that of a groove. At heavy loads the impressive result was that, when elastic deformation was considered, the bump or groove essentially disappeared. These preliminary results show that micro-EHL can be studied easily by using this new powerful tool. An exhaustive study can now be performed to control the effect of load, sliding speed, and roughness

wavelength and height on the stress field. Temperature increases in the film and on the surfaces should also be included to better understand scuffing.

APPENDIX

Derivation of Jacobian Factors

Calculation of df_i/dP_j. - Roelands' viscosity is expressed as

$$\bar{\eta}_i = \exp\left\{(\ln \eta_0 + 9.67) \times \left[-1 + \left(1 + 5.1\times10^{-9}\, p_H P_i\right)^{Z'}\right]\right.$$

where Z' is the Roelands pressure parameter, equal to 0.69 in this study. By writing now $d\eta_i/dP_j = \dot{\eta}$, we have

$$\dot{\eta} = 5.1\times10^{-9}\, p_H[\ln \eta_0 + 9.67] \times \left[1 + 5.1\times10^{-9}\, p_H P_i\right]^{Z'-1} \bar{\eta}_i\, k_{ij}$$

where k_{ij} is the Kronecker symbol

$$k_{ij} = 1 \quad \text{if} \quad i = j$$

$$k_{ij} = 0 \quad \text{if} \quad i \neq j$$

The density $\bar{\rho}$ is written as

$$\bar{\rho}_i = 1 + \frac{0.6\times10^{-9}\, p_H P_i}{1 + 1.7\times10^{-9}\, p_H P_i}$$

which leads to

$$\frac{d\bar{\rho}_i}{dP_j} = \dot{\rho} = \frac{0.6\times10^{-9}\, p_H}{\left(1 + 1.7\times10^{-9}\, p_H P_i\right)^2} k_{ij}$$

In the appendix of Houpert and Hamrock (1985), $d(dP/dX)/dP_j$ has been expressed and can be written for simplicity as

$$\frac{d\left(\frac{dP}{dX}\right)_i}{dP_j} = \dot{P}$$

By definition of D_{ij} we have

$$\frac{dH_i}{dP_j} = \dot{H} = D_{ij}$$

For simplicity, the subscript i will be omitted when possible in what follows.

From the definition of $\bar{\tau}_0$ we have

$$\frac{d\bar{\tau}_0}{dP_j} = \dot{\tau}_0 = \frac{ap_H}{\tau_{0,\ell}} \exp\left(\frac{-ap_H P_i}{\tau_{0,\ell}}\right) k_{ij}$$

Using the dimensionless variables we have

$$T = C_1 \frac{\frac{dP}{dX} H}{\bar{\tau}_0}$$

$$S = \frac{C_2}{1 + \frac{A}{2}} \frac{\bar{\eta}}{H\bar{\tau}_0}$$

which leads to

$$\frac{dT_i}{dP_j} = \dot{T} = C_1 \frac{\left[\left(\dot{P}H + \dot{H}\frac{dP}{dX}\right)\bar{\tau}_0 - \dot{\tau}_0 \frac{dP}{dX} H\right]}{\bar{\tau}_0^2}$$

$$\frac{dS_i}{dP_j} = \dot{S} = \frac{C_2}{1 + \frac{A}{2}} \left[\frac{\dot{\eta}H\bar{\tau}_0 - \bar{\eta}\left(\dot{H}\bar{\tau}_0 - \dot{\tau}_0 H\right)}{\left(H\bar{\tau}_0\right)^2}\right]$$

We can now define a series of new variables

$$B_1 = \frac{AST}{2 \sinh\left(\frac{T}{2}\right)}; \quad \frac{d(B_1)}{dP_j} = \dot{B}_1$$

$$\dot{B}_1 = \frac{A}{2}\left[\frac{(\dot{S}T + S\dot{T}) \sinh\left(\frac{T}{2}\right) - \dot{T} \cosh\left(\frac{T}{2}\right) ST}{\left[\sinh\left(\frac{T}{2}\right)\right]^2}\right]$$

$$B_2 = \left(1 + B_1^2\right)^{1/2}; \quad \frac{d(B_2)}{dP_j} = \dot{B}_2; \quad \dot{B}_2 = \frac{\dot{B}_1 B_1}{B_2}$$

$$B_3 = \frac{\sinh\left(\frac{T}{2}\right)}{\frac{T}{2}} - \cosh\left(\frac{T}{2}\right) + \frac{T^2}{12}$$

$$\dot{B}_3 = \frac{dB_3}{dP_j} = \left[\frac{\frac{1}{2}\cosh\left(\frac{T}{2}\right)\frac{T}{2} - \frac{1}{2}\sinh\left(\frac{T}{2}\right)}{\left(\frac{T}{2}\right)^2} - \frac{1}{2}\sinh\left(\frac{T}{2}\right) + \frac{T}{6}\right]\dot{T}$$

$$B_4 = \frac{-12H}{\frac{dP}{dX}} B_3; \quad \frac{d(B_4)}{dP_j} = \dot{B}_4$$

$$\dot{B}_4 = -12\,\frac{\left(\dot{H}\,\frac{dP}{dX} - H\dot{P}\right)}{\left(\frac{dP}{dX}\right)^2} - \frac{12\,H}{\frac{dP}{dX}}\,\dot{B}_3$$

Using dimensionless variables, e may be written as

$$e = B_4\,\frac{\bar{\tau}_o^2}{C_1^2}$$

leading to

$$\frac{de_i}{dP_j} = \dot{e} = \frac{1}{C_1^2}\left(\dot{B}_4\bar{\tau}_o^2 + 2\bar{\tau}_o\dot{\bar{\tau}}_o B_4\right)$$

From the definition of f, we have

$$f = H^3\,\frac{dP}{dX} - \frac{K\bar{n}\left(H - \frac{\bar{\rho}_e H_e}{\bar{\rho}}\right)}{B_2} + e$$

The derivation of f is now easy:

$$\frac{df}{dP_j} = \dot{f} = 3H^2\dot{H}\,\frac{dP}{dX} + H^3\dot{P}$$

$$- K\,\frac{1}{B_2}\left[\dot{n}\left(H - \frac{\bar{\rho}_e H_e}{\bar{\rho}}\right) + \bar{n}\left(\dot{H} - \frac{\bar{\rho}_e H_e\dot{\rho}}{\bar{\rho}^2}\right)\right]$$

$$+ \frac{K\dot{B}_2\bar{n}\left(H - \frac{\rho_e H_e}{\bar{\rho}}\right)}{B_2^2} + \dot{e}$$

Calculation of df/dH_0. - Using the same notation we may write

$$\frac{dH}{dH_0} = \dot{H} = 1$$

$$\dot{n} = \dot{\rho} = \dot{P} = 0$$

and the previous formulations can be kept.

Calculation of $df/d(\rho_e H_e)$. - From the definition of f, we have

$$\frac{df}{d(\rho_e H_e)} = \frac{K\bar{n}}{\bar{\rho}B_2}$$

APPENDIX

References

Bair, S. and Winer, W.O. (1978), "Rheological Response of Lubricants in EHD Contacts," Paper V (ii), Proc. of the 5th Leeds-Lyon Symposium, pp. 162-169.

Berthe, D., Flamand, L., and Houpert, L. (1978), "Rheological Parameters of a Lubricant Under High Speed Conditions," Paper VI (ii), Proc. of the 5th Leeds-Lyon Symposium. Butterworths, Guilford, England.

Berthe, D., Houpert, L., and Flamand, L. (1979), "Thermal Effects in EHD Contacts for Different Rheological Behaviours of the Lubricant," Proc. of the 6th Leeds-Lyon Symposium. Butterworths, Guilford, England.

Cheng, H.S. (1983), "Micro Elastohydrodynamic Lubrication," Tribology in the 80's, NASA CP-2300, vol. II, pp. 615-639.

Cusano, C. and Wedeven, L.D. (1983), "The Influence of Surface Dents and Grooves in Traction in Sliding EHD Point Contacts," ASLE Trans., vol. 26, no. 3, pp. 306-310.

Dyson, A. (1976), "A Failure of EHD Lubrication of Circumferentially Ground Discs," J. Instr. Mech. Engr., vol. 190, 52/76, pp. 699-711.

Eyring, H. (1936), "Viscosity, Plasticity, and Diffusion as Examples of Absolute Reaction Rates," J. Chem. Phys., vol. 4, pp. 283-291.

Hamrock, B.J. and Jacobson, B.O. (1984), "Elastohydrodynamic Lubrication of Line Contacts," Trans. ASLE, vol. 27, no. 4, pp. 275-287.

Hirst, W. and Moore, A.J. (1974), "Non-Newtonian Behavior in Elastohydrodynamic Lubrication," Proc. R. Soc. London., Ser. A, vol. 337, pp. 101-121.

Houpert, L., Flamand, L., and Berthe, D. (1981), "Rheological and Thermal Effects in a Lubricated EHD Contact," J. Lubr. Technol. (ASME), vol. 103, pp. 526-533.

Houpert, L. (1985a), "Fast Numerical Calculations of EHD Sliding Traction Forces; Application to Rolling Bearings," J. Tribology (ASME), vol. 107, pp. 234-240.

Houpert, L. (1985b), "New Results of Traction Force Calculations in Elastohydrodynamic Contacts," J. Tribology (ASME), vol. 107, pp. 241-248.

Houpert, L. and Hamrock, B.J. (1985), "Fast Approach for Calculating Film Thickness and Pressures in Elastohydrodynamic Lubricated Contacts at High Loads," ASME Paper 85-TRIB-42, 1985.

Ioannides, E. and Harris, T. (1985), "A New Fatigue Life Model for Rolling Bearings," J. Tribology (ASME), vol. 107, no. 3, pp. 367-378.

Johnson, K.L. and Greenwood, J.A. (1980), "Thermal Analysis of an Eyring Fluid in Elastohydrodynamic Tractions," Wear, vol. 61, pp. 353-374.

Johnson, K.L. and Tevaarwerk, J.L. (1977), "Shear Behaviour of EHD Oil Films," Proc. R. Soc. London, Ser. A, vol. 356, p. 215.

Okamura, H. (1982), "A Contribution to the Numerical Analysis of Isothermal Elastohydrodynamic Lubrication," Tribology of Reciprocating Engines. Proceedings of the 9th Leeds-Lyon Symposium on Tribology, Butterworths, Guilford, England, pp. 313-320.

Ten Napel, W.E., Klein Meuleman, P., Lubrecht, A.A., Houpert, L., and Bosma, R. (1985), "Traction in Elastohydrodynamic Lubrication at Very High Contact Pressure," Post-session paper presented at the 1985 Eurotrib Conference.

TABLE I. - IMPORTANT EQUATIONS FOR NONLINEAR VISCOUS AND LINEAR VISCOUS MODELS

	Nonlinear viscous	Linear viscous
Rheology	$\frac{d}{dZ}\left(\frac{u}{u_a}\right) = \frac{1}{S}\sinh\left(\frac{\tau}{\tau_o}\right)$	$\frac{d}{dZ}\left(\frac{u}{u_a}\right) = \frac{1}{S}\left(\frac{\tau}{\tau_o}\right)$
Equilibrium	$T = \frac{d}{dZ}\left(\frac{\tau}{\tau_o}\right)$	$T = \frac{d}{dZ}\left(\frac{\tau}{\tau_o}\right)$
Shear rate distribution	$\frac{d}{dZ}\left(\frac{u}{u_a}\right) = \frac{1}{S}\sinh\left[T\,(Z - 0.5)\right] + \sinh^{-1}\left[\frac{CST/2}{\sinh\,(T/2)}\right]$	$\frac{d}{dZ}\left(\frac{u}{u_1}\right) = \frac{T}{S}\,(Z - 0.5) + A$
Shear stress distribution	$\frac{\tau}{\tau_o} = T\,(Z - 0.5) + \sinh^{-1}\left(\frac{AST/2}{\sinh\,(T/2)}\right)$	$\frac{\tau}{\tau_o} = T(Z - 0.5) + AS$
Velocity distribution	$\frac{u}{u_a} = 1 + A + \frac{2}{ST}\sinh\left[\frac{T}{2}\,(Z - 1)\right] \times \sinh\left\{\frac{TZ}{2} + \sinh^{-1}\left[\frac{AST/2}{\sinh\,(T/2)}\right]\right\}$	$\frac{u}{u_a} = 1 + AZ + \frac{TZ\,(Z - 1)}{2S}$
Reynolds	$f = H^3\frac{dP}{dX} - \frac{K\bar{n}\,(H - \rho_e H_e/\rho)}{\left\{1 + [AST/2\,\sinh\,(T/2)]^2\right\}^{1/2}} + e$ $e = -\frac{6\pi H^2\tau_o}{E'WT}\left[\frac{\sinh\,(T/2)}{(T/2)} - \cosh\left(\frac{T}{2}\right) + \frac{T^2}{12}\right]$	$f = H^3\frac{dP}{dX} - K\bar{n}\left(H - \frac{\rho_e H_e}{\rho}\right)$

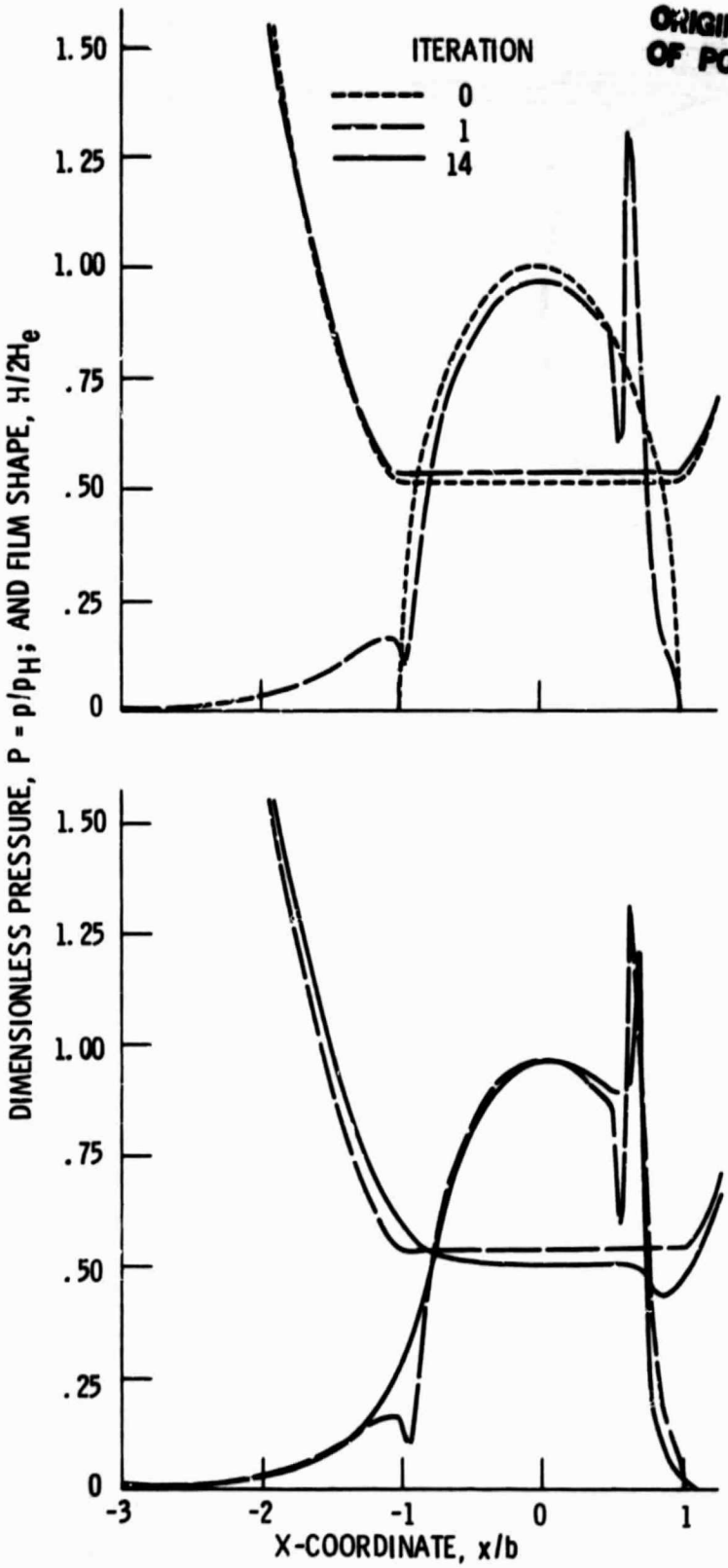

Fig. 1 Pressure and film profiles at iterations 0, 1, and 14. Barus' pressure-viscosity formula. Dimensionless load, speed, and materials parameters held fixed at $W = 2 \times 10^{-5}$, $U = 1 \times 10^{-11}$, and $G = 5007$. (From Houpert and Hamrock (1985).)

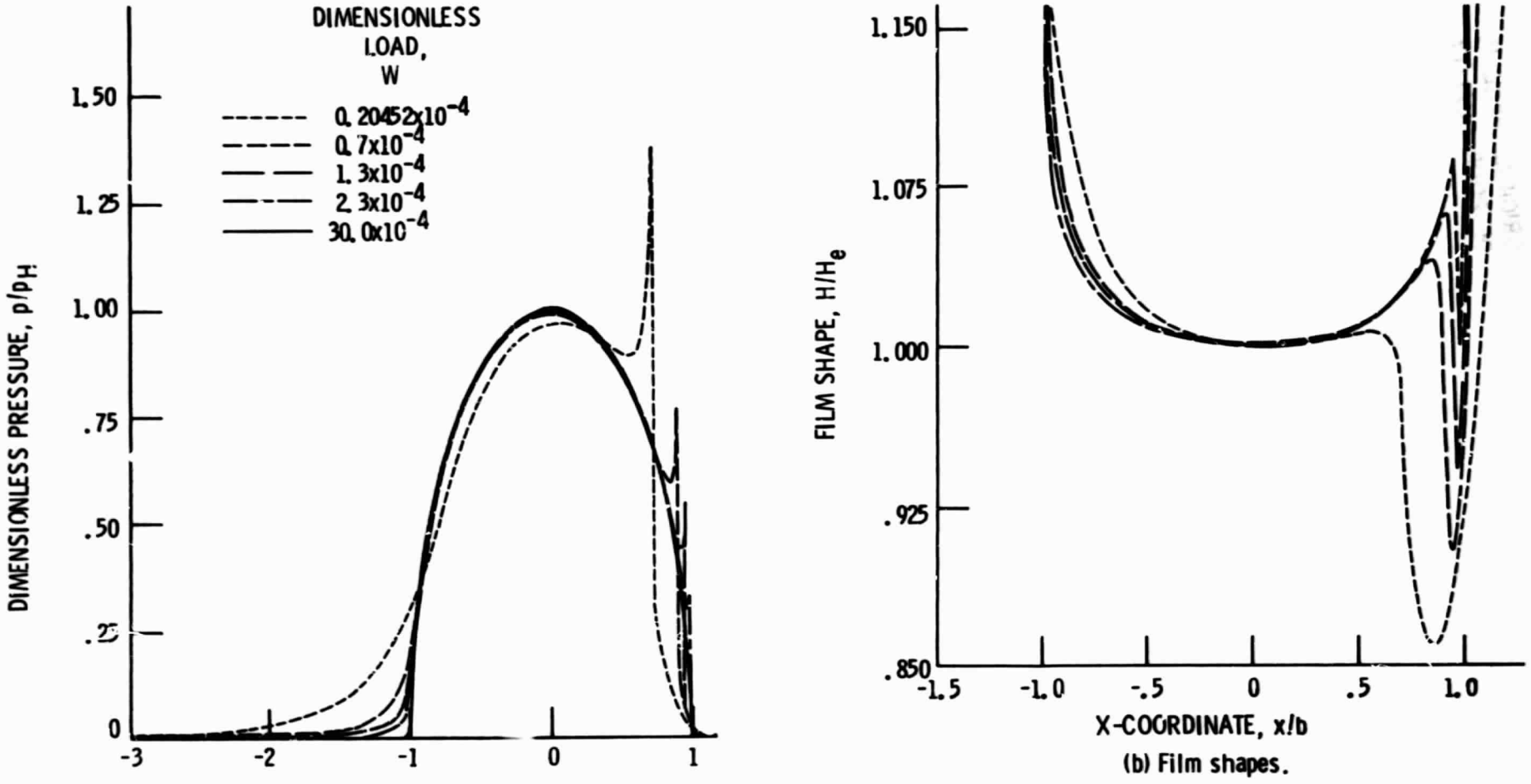

(a) Pressure profiles.

(b) Film shapes.

Fig. 2 Dimensionless pressure and film profiles for varying dimensionless loads. Roelands' pressure-viscosity formula. Dimensionless speed and materials parameters held fixed at $U = 1x10^{-11}$ and $G = 5007$. (From Houpert and Hamrock (1985).)

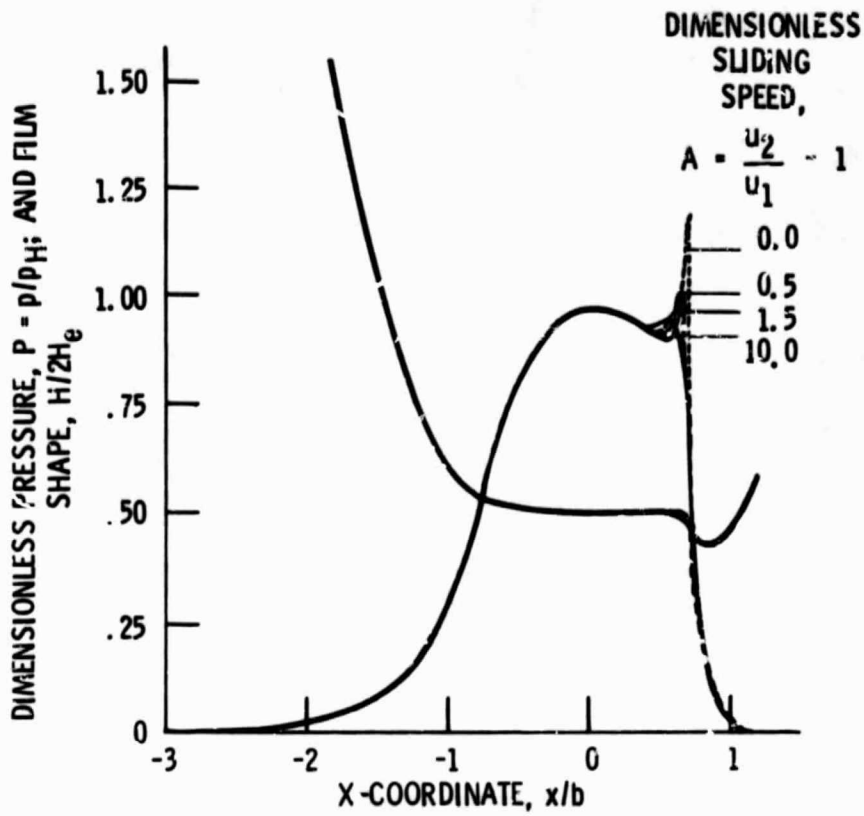

Fig. 3 Dimensionless pressure and film profiles for varying dimensionless sliding speeds. Dimensionless load, speed, and materials parameters held fixed at $W = 2 \times 10^{-5}$, $U = 1 \times 10^{-11}$, and $G = 5007$.

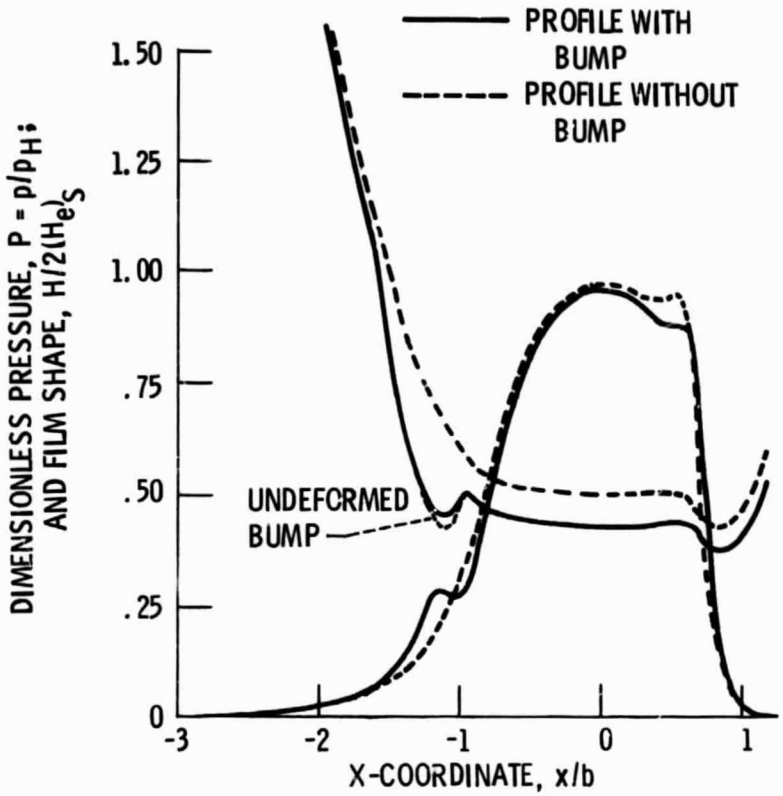

Fig. 4 Dimensionless pressure and film profiles without and with a bump in inlet region. Dimensionless load, speed, materials, and sliding speed parameters held fixed at $W = 2 \times 10^{-5}$, $U = 1 \times 10^{-11}$, $G = 5007$, and $A = 10$. Bump depth, 0.1×10^{-6} m; bump width, 0.5×10^{-4} m.

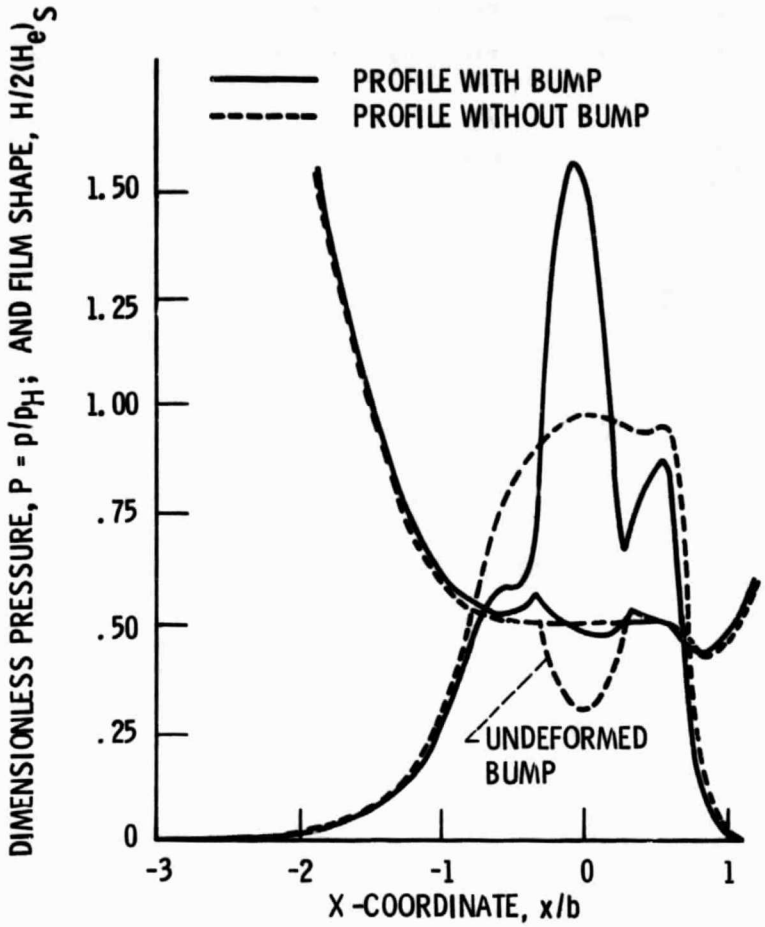

Fig. 5 Dimensionless pressure and film profiles without and with a bump in center of contact. Dimensionless load, speed, materials, and sliding speed parameters held fixed at $W = 2\times10^{-5}$, $U = 1\times10^{-11}$, $G = 5007$, and $A = 10$. Bump depth, 0.1×10^{-6}m; bump width, 0.5×10^{-4}m.

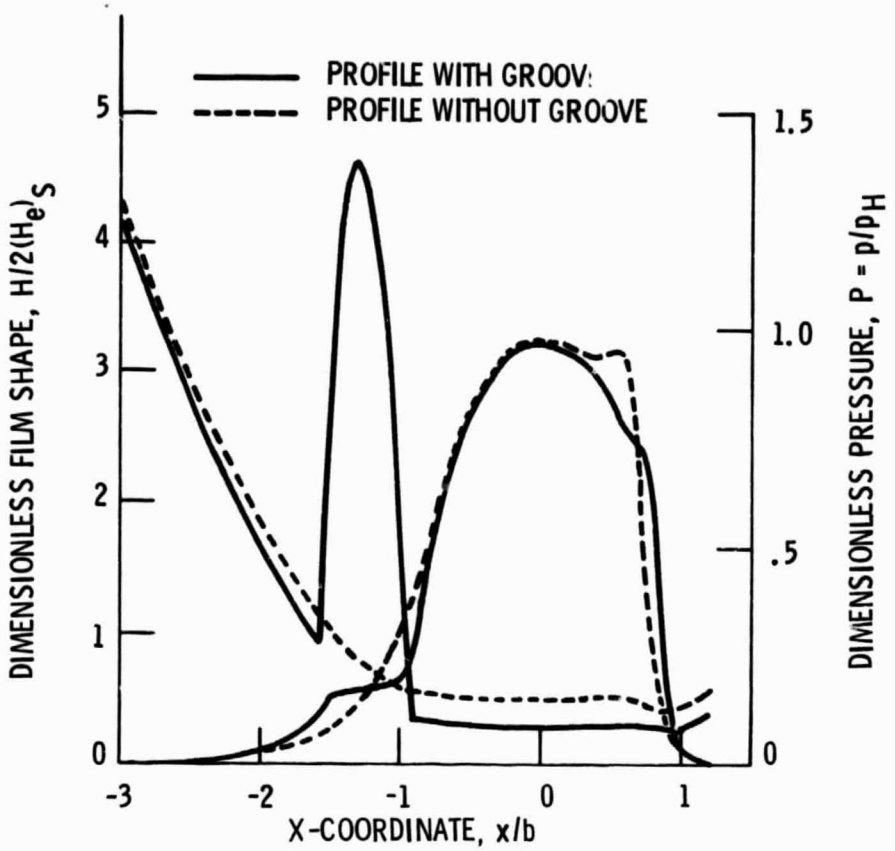

Fig. 6 Dimensionless pressure and film profiles without and with a groove in inlet region. Dimensionless load, speed, materials, and sliding speed parameters held fixed at $W = 2\times10^{-5}$, $U = 1\times10^{-11}$, $G = 5007$, and $A = 10$. Groove depth, 2×10^{-6} m; groove width, 0.5×10^{-4} m.

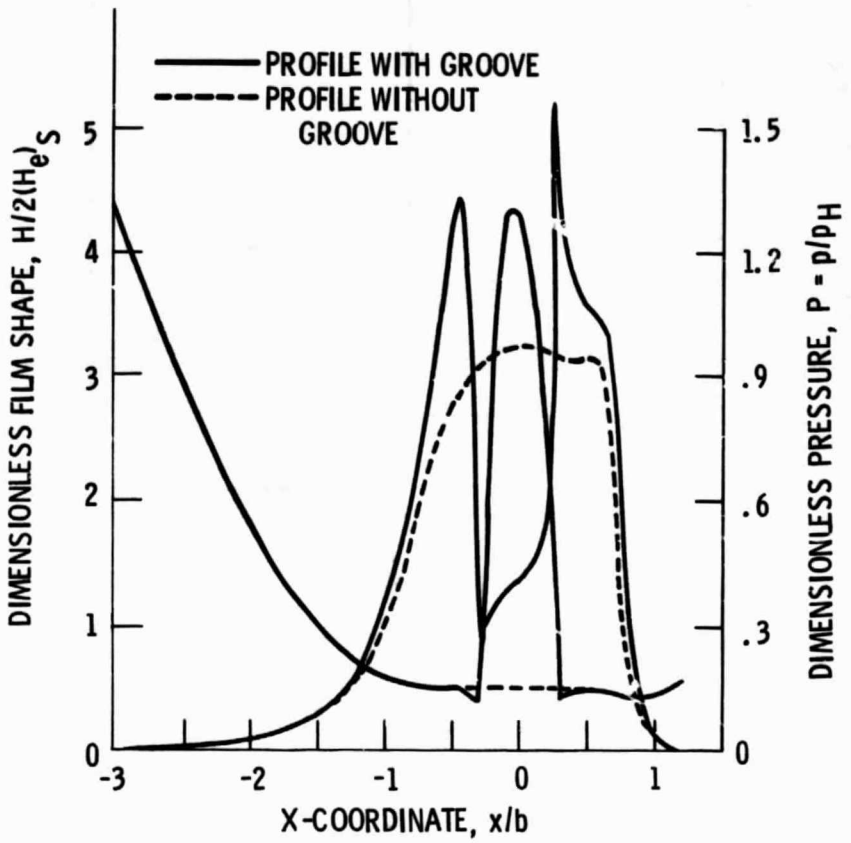

Fig. 7 Dimensionless pressure and film profiles without and with a groove in center of contact. Dimensionless load, speed, materials, and sliding speed parameters held fixed at $W = 2\times10^{-5}$, $U = 1\times10^{-11}$, $G = 5007$, and $A = 10$. Groove depth, 2×10^{-6} m; groove width, 0.5×10^{-4} m.

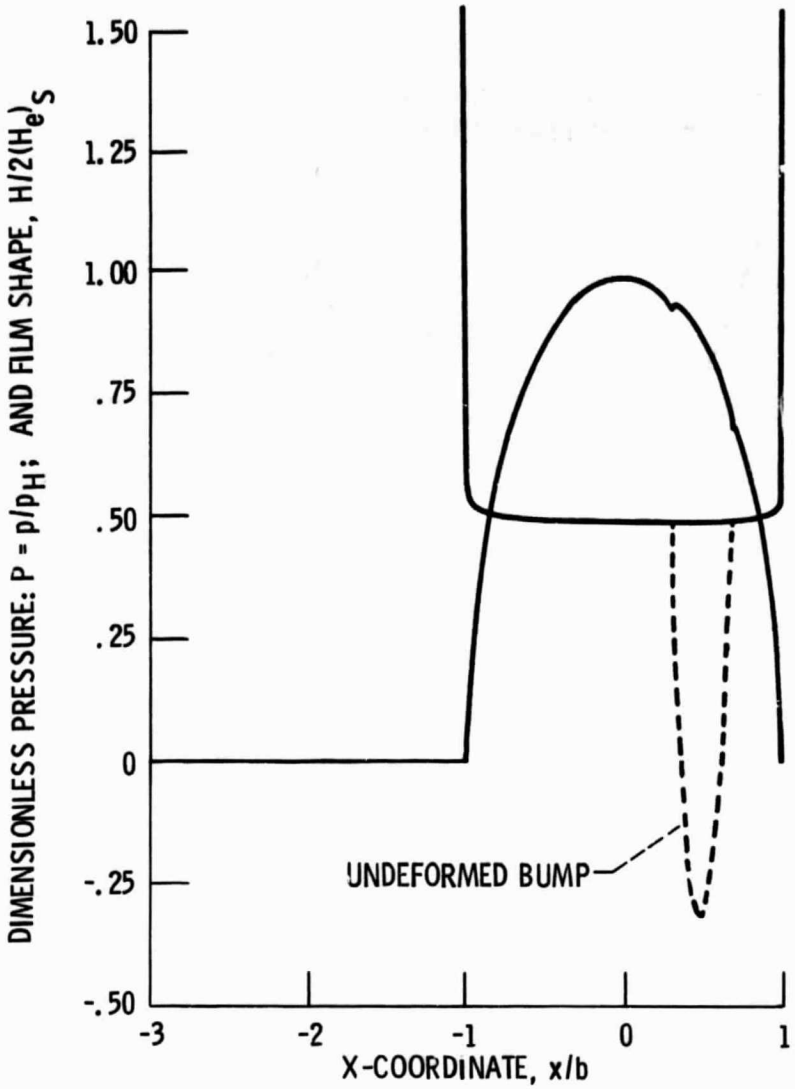

Fig. 8 Dimensionless pressure and film profiles with bump in heavily loaded contact. Dimensionless load, speed, materials, and sliding speed parameters held fixed at $W = 3\times10^{-3}$, $U = 1\times10^{-11}$, $G = 5007$, and $A = 0.1$. Bump depth, 1.4×10^{-7} m; bump width, 3.88×10^{-4} m.

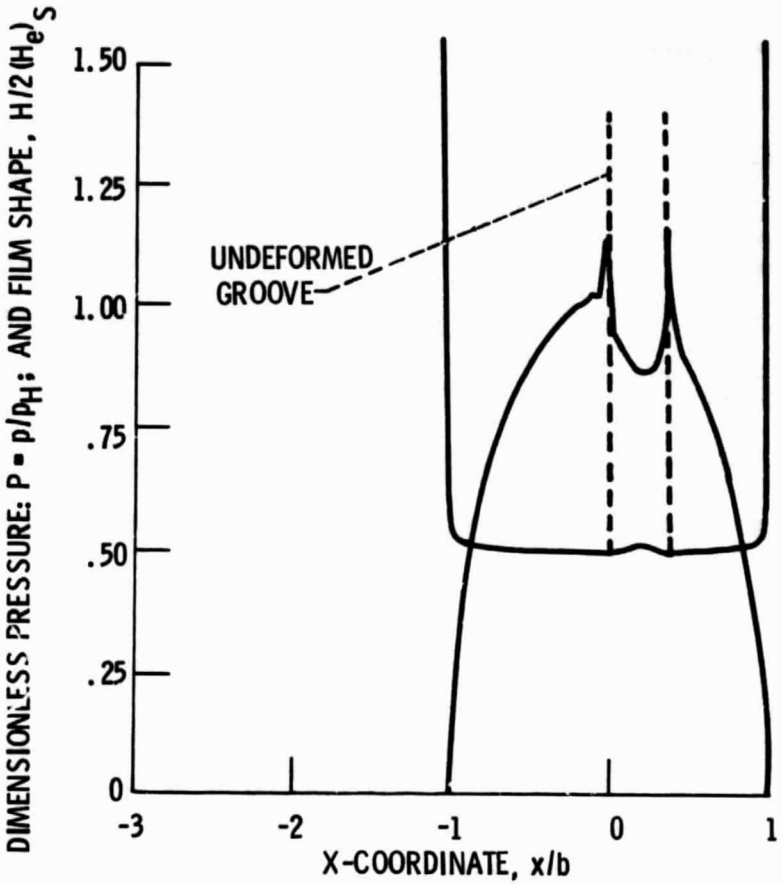

Fig. 9 Dimensionless pressure and film profiles with groove in heavily loaded contact. Dimensionless load, speed, materials, and sliding speed parameters held fixed at $W = 3\times10^{-3}$, $U = 1\times10^{-11}$, $G = 5007$, and $A = 0.1$. Groove depth, 1.48×10^{-6} m; groove width, 3.88×10^{-4} m.

1. Report No.	2. Government Accession No.	3. Recipient's Catalog No.
NASA TM-87097		

4. Title and Subtitle	5. Report Date
Elastohydrodynamic Lubrication Calculations Used as a Tool to Study Scuffing	6. Performing Organization Code: 505-33-62

7. Author(s)	8. Performing Organization Report No.
L.G. Houpert and B.J. Hamrock	E-2658
	10. Work Unit No.

9. Performing Organization Name and Address	11. Contract or Grant No.
National Aeronautics and Space Administration Lewis Research Center Cleveland, Ohio 44135	13. Type of Report and Period Covered: Technical Memorandum

12. Sponsoring Agency Name and Address	14. Sponsoring Agency Code
National Aeronautics and Space Administration Washington, D.C. 20546	

15. Supplementary Notes

Prepared for the 12th Leeds-Lyon Symposium on Tribology, Lyon, France, September 3-6, 1985.

16. Abstract

A new Reynolds equation is developed that takes into account the nonlinear viscous behavior of the fluid. The new Reynolds equation considers the nonlinear viscous fluid model of Eyring, the equilibrium equation, the constant mass flow, and the kinematic boundary condition. The new Reynolds equation and the elasticity equation are solved simultaneously by using a system approach and a Newton-Raphson technique. Comparisons are made with results obtained from the classical Reynolds equation. The effects of sliding speed and introducing a bump or a groove within the conjunction are studied. Results are shown for both moderate and heavy loads.

17. Key Words (Suggested by Author(s))	18. Distribution Statement
Scuffing; Elastohydrodynamic lubrication; Surface texture; Non-Newtonian fluid effects	Unclassified - unlimited STAR Category 37

19. Security Classif. (of this report)	20. Security Classif. (of this page)	21. No. of pages	22. Price*
Unclassified	Unclassified		

*For sale by the National Technical Information Service, Springfield, Virginia 22161